

## Nonlinear response history analysis and collapse mode study of a wind turbine tower subjected to tropical cyclonic winds

Kaoshan Dai<sup>\*1,2</sup>, Chao Sheng<sup>1</sup>, Zhi Zhao<sup>1</sup>, Zhengxiang Yi<sup>1</sup>,  
Alfredo Camara<sup>3</sup> and Girma Bitsuamlak<sup>4</sup>

<sup>1</sup>State Key Laboratory of Disaster Reduction in Civil Engineering, Tongji University, Shanghai, China

<sup>2</sup>Key Laboratory of Energy Engineering Safety and Disaster Mechanics, Ministry of Education  
(Sichuan University) Chengdu, China

<sup>3</sup>Department of Civil Engineering, City University London, UK

<sup>4</sup>Department of Civil and Environmental Engineering, University of Western Ontario, Canada

(Received December 17, 2016, Revised June 29, 2017, Accepted June 30, 2017)

**Abstract.** The use of wind energy resources is developing rapidly in recent decades. There is an increasing number of wind farms in high wind-velocity areas such as the Pacific Rim regions. Wind turbine towers are vulnerable to tropical cyclones and tower failures have been reported in an increasing number in these regions. Existing post-disaster failure case studies were mostly performed through forensic investigations and there are few numerical studies that address the collapse mode simulation of wind turbine towers under strong wind loads. In this paper, the wind-induced failure analysis of a conventional 65 m hub high 1.5-MW wind turbine was carried out by means of nonlinear response time-history analyses in a detailed finite element model of the structure. The wind loading was generated based on the wind field parameters adapted from the cyclone boundary layer flow. The analysis results indicate that this particular tower fails due to the formation of a full-section plastic hinge at locations that are consistent with those reported from field investigations, which suggests the validity of the proposed numerical analysis in the assessment of the performance of wind-farms under cyclonic winds. Furthermore, the numerical simulation allows to distinguish different failure stages before the dynamic collapse occurs in the proposed wind turbine tower, opening the door to future research on the control of these intermediate collapse phases.

**Keywords:** wind turbine tower; tropical cyclone; wind load; buckling analysis; structural collapse; failure mode

### 1. Introduction

In recent decades, the use of wind energy resources has developed rapidly worldwide (WWEA 2016). Structural and environmental issues associated with the development of wind energy become one of research interests (Spagnoli and Montanari 2013, Dai *et al.* 2015, Sultania and Manuel 2016). Wind turbine (WT) towers are vulnerable to structural failures induced by tropical cyclone (TC) and strong winds (Ishihara *et al.* 2005, Chen *et al.* 2015, Chen and Xu 2016). International standards such as International Electrotechnical Commission (IEC) 61400 (IEC

---

\*Corresponding author, Associate professor, E-mail: [kdai@tongji.edu.cn](mailto:kdai@tongji.edu.cn)

61400-3 2005) and Germanischer Lloyd (GL) Guideline (Lloyd 2005) are mostly adopted for WT design. However, previous references are not sufficiently detailed to accurately consider extreme loading conditions such as TC. Recently, a design code (GB/T 31519-2015 2015) was published in China for application in WTs in coastal and offshore wind farms under the typhoon conditions. There is an increasing concern on the safety of WT farms in the future due to the increasing risk of extreme weather conditions triggered by the climate change (Field 2012).

Several field case studies on WT tower failures have been reported (Ishihara *et al.* 2005, Chou and Tu 2011, Chen *et al.* 2015, Chen and Xu 2016). In addition to field investigations, a rigorous numerical analysis is an effective approach to assess possible failure causes and improve the structural design of wind turbine towers. Typically, static (pseudo-dynamic) failure analyses were performed in these studies (Chou and Tu 2011, Lee and Bang 2012, Chen *et al.* 2015). However, the collapse of WT towers under strong winds is a complex dynamic problem; therefore, time-history analyses were preferred (Ishihara *et al.* 2005, Wang *et al.* 2013, Zhang *et al.* 2014). The finite element (FE) method is a reliable numerical tool for the assessment of WT under extreme loading conditions (Lavassas *et al.* 2003, Dai *et al.* 2015) and a detailed modeling technique is required in order to study the failure mechanisms. Nevertheless, few studies focused on the entire failure process or propose a reliable failure mode analysis of WT towers subjected to strong winds, which is of interest to the wind energy industry.

The combination of a detailed structural model and a reliable tropical cyclone wind field is required to accurately model WT tower failure mode. A significant number of works have addressed the wind field parameters that are necessary to describe the wind field model, such as the extreme wind speed, wind profile, turbulence intensity, turbulence integral scale and turbulence power spectrum, among others (Choi 1978, Vickery *et al.* 2009). Comparing between the tropical cyclone boundary layer and the atmospheric boundary layer, TC presents a characteristic strong wind speed combined with high levels of turbulence and sudden changes of the wind direction (Li *et al.* 2013, GB/T 31519-2015 2015). Considering these characteristics in the structural response of wind turbine towers under typhoon wind actions seems to be important, but few studies have addressed these problems with sufficient detail.

In this paper, a typical 1.5-MW WT supporting tower was modeled in ABAQUS (ABAQUS 2013) with a rigorous consideration of structural details in the tower and the wind field. A turbulence numerical simulation method based on the consistent discrete random flow generation (CDRFG) was used to generate stochastic along-wind time-history cyclone velocity field records with state-of-the-art cyclone wind characteristics. The WT blade loading was estimated based on the blade element momentum (BEM) theory (Hansen 2008). A series of dynamic nonlinear response history analyses were conducted to investigate the effect of inflow directions under different levels of extreme winds and structural performances at different stages until collapse was observed. In addition, linear eigenvalue buckling analyses were performed and compared to the nonlinear dynamic analysis.

## **2. WT tower modeling and wind load simulation**

### *2.1 FE modeling and modal analysis*

#### *2.1.1 FE modeling*

The WT under consideration is a S70/1500 horizontal axial wind turbine with 1.5-MW capacity

and three blades. The supporting structure is a 61.8 m hollow tubular steel tower ( $H=61.8$  m) with a hub height  $H'=65$  m, as shown in Fig. 1. To facilitate transportation, the tower was divided into three components connected by four flanges at approximately 13 and 34 m height, as well as at the top and bottom sections, respectively. The entire tower was welded with 22 segments with different wall thicknesses varying from 25 mm at the base to a minimum of 10 mm at the top (Fig. 2). The thickness of the top segment reached 14 mm to facilitate the support of the blades, hub and cabin of the WT. The fore-aft direction is associated with the axis “X” and the side-side direction is defined as the axis “Z”. The details of this WT tower are depicted in Fig. 2.

The FE model of the WT is defined in ABAQUS 6.13\_1 (ABAQUS 2013). The model was focused on the collapse mode investigation of this WT tower. The 22 segments of the hollow thin-wall steel tower welded by 19 welding lines and 2 bolted flanges were all simulated by standard linear reduced-integration 3D shell element “S4R”. The flanges at 13 m and 34 m heights (“F” in Fig. 2) represent internal platforms. The mass and stiffness contributions of these platforms were considered by increasing the thickness of the corresponding ring of shell elements. The wall segments were modeled using a tetrahedral sweep grid technique. The exception is the bottom segment where the meshing was performed with a quad-dominated free grid technique to allow introducing the real geometry of the door cut. A mesh-sensitivity analysis was conducted in order to accurately capture the occurrence of initial plastic hinges.

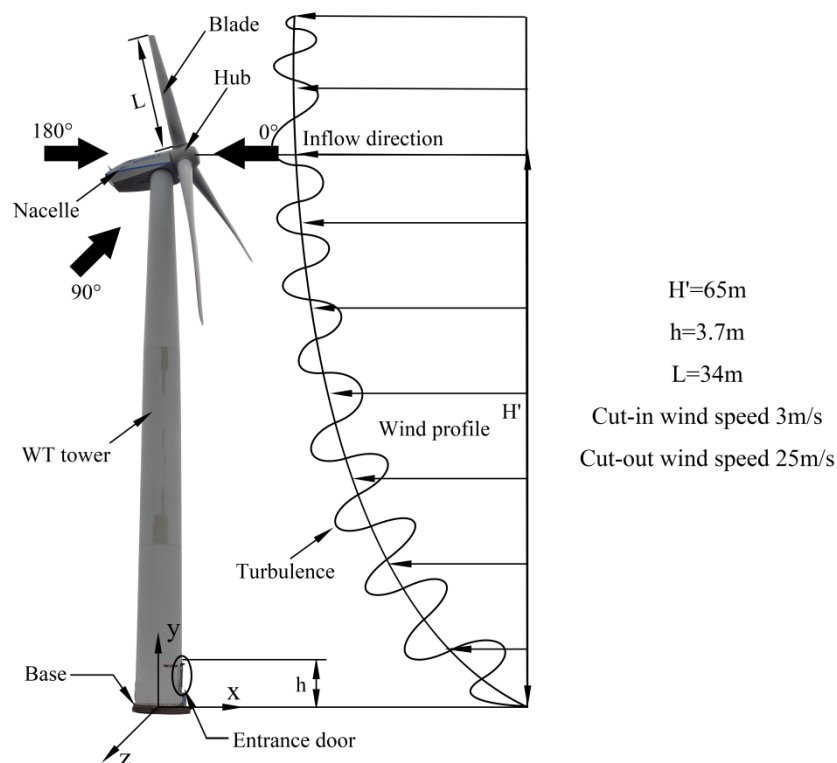


Fig. 1 The prototype of S70/1500 horizontal axial wind turbine under wind loads

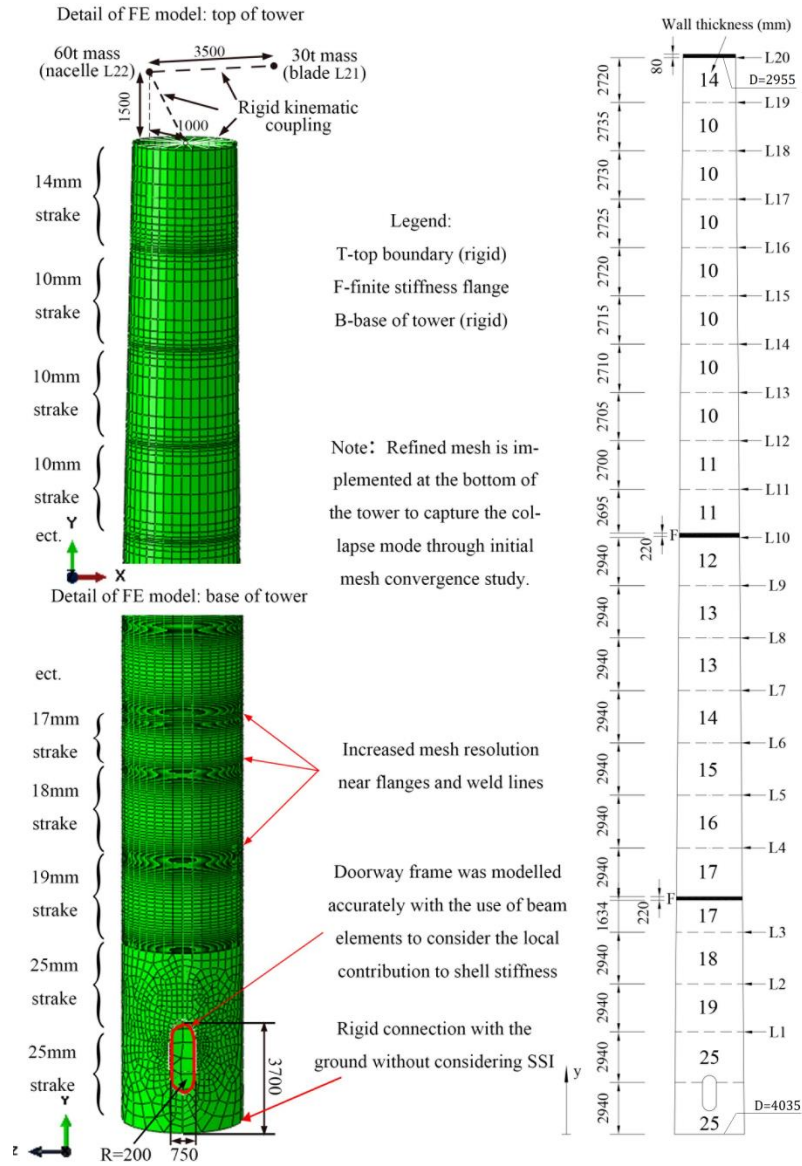


Fig. 2 Details of the WT tower and its FE model (Unit: mm)

As a result, the mesh was refined close to the door and near the flanges and weld lines, as illustrated in Fig. 2. The peripheral reinforcing of the door was modeled by means of beam elements with linear interpolation that were tied to the corresponding shell elements. The WT supporting tower was made of S355 steel, with a yield stress of 355 MPa, a Poisson's ratio of 0.3 and a density of 7850 kg/m<sup>3</sup>. The constitutive relationship of the steel was defined with an elastic-plastic nonlinear model that includes a plastic hardening of 0.1% of 210 Gpa. This small hardening was selected after the study conducted in (Sadowski *et al.* 2016). The wall at the connection with the foundation was considered to be rigidly fixed, hence ignoring the effect of soil

- structure interaction.

The blades, hub, and nacelle were modeled as point lumped masses. The total mass on the top of the supporting tower was estimated as 90,000 kg, which was distributed into the point mass of the blade including the hub (30,000 kg) and the nacelle (60,000 kg). These masses were determined after the model updating based on the field dynamic characteristics test results of this WT given in (Dai *et al.* 2015). The influence of the rotary inertia of the blades on the initial vibration modes of the structure was neglected based on preliminary analyses. A rigid body kinematic coupling was implemented to define the connection between the mass points representing the 'blade' and the 'nacelle'. This connection was also established between the mass points and the shell nodes on the top of the tower ("T" in Fig. 2). This simplification modeling approach helps focus the study on tower structure itself instead of the blade-tower system, which should be feasible since blade modal mass participation factor is small and the fundamental tower bending mode is usually dominant as indicated in Patil *et al.* (2016). The dynamic implicit algorithm built in the ABAQUS package was adopted in response history analyses.

### 2.1.2 Modal analysis

The vibration modes and the associated frequencies of the WT tower were extracted and presented in Fig. 3 for different orientations of the nacelle. The fundamental period involving the global flexure of the wall has a frequency of 0.49 Hz (2.04s), matching very closely the previous field testing results, with only 1.5% difference (Dai *et al.* 2015). After the first global flexure mode in the X-direction, the first global flexure mode shape in the Z-direction is similar to that in the X-direction, with a frequency of 0.49 Hz. The second global flexure frequencies in the horizontal directions are 4.3 Hz (X-direction) and 4.4 Hz (Z-direction), respectively. These are followed by local flexure modes of the tower wall. The first torsional frequency is 7.36 Hz and the first vertical (Y-direction) modal frequency is 10.97 Hz. By adjusting the orientation  $\omega$  of the nacelle relative to the doorway, a total of 100 modal analyses were conducted and the natural frequencies of the tower are summarized in Fig. 3. Negligible differences were observed in the vibration frequencies for all the modes below 50 Hz by changing the orientation angles  $\omega$ .

## 2.2 WT wind load estimation

### 2.2.1 Cyclone wind velocity field simulation

Strong winds are one of the primary causes of WT failures in TC-prone regions. TC wind conditions are characterized by strong wind speeds, high turbulence levels and sudden changes of the wind direction, which induce a potentially violent structural response that could lead to the failure of WT towers (Li *et al.* 2013). The typical parameters describing the cyclone boundary layer had been reported in (Shiau and Chen 2001, An *et al.* 2012). In this study, the characteristic parameters adopted for TC loading evaluation were summarized in Table 1. The detailed discussion on these parameters can be referred to Han *et al.* (2014). The consistent discrete random flow generation (CDRFG) method was used in this study to simulate the wind velocity field replicating high levels of turbulence of TCs with the targeted Von Karman's theoretical spectrum. The CDRFG method generates a turbulent velocity field that satisfies the targeted turbulent spectra as well as spatial and time correlations based on the discretization of the velocity power spectra. Further details of this procedure can be found in Aboshosha *et al.* (2015).

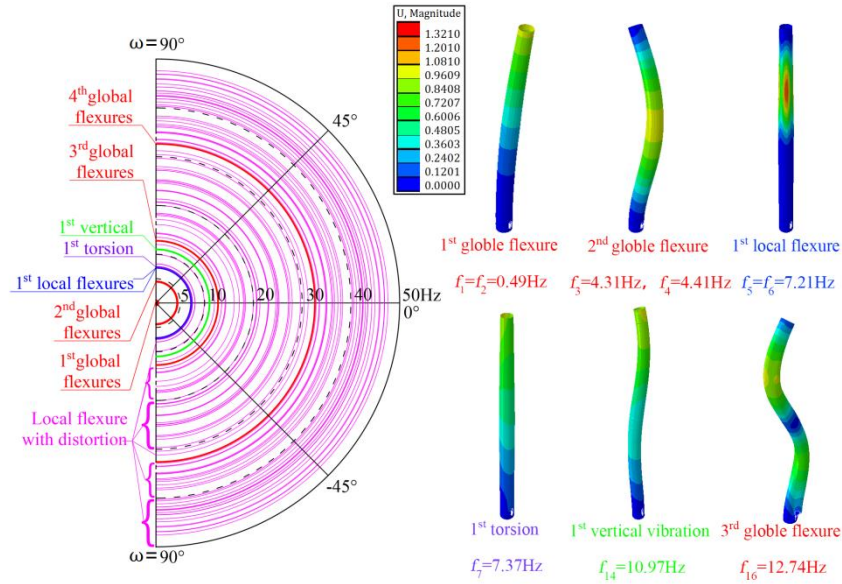


Fig. 3 Polar plot of the first 100 frequencies  $f$  (Hz) against the nacelle orientation ( $^\circ$ ) with several typical vibration mode shapes (the left side of the polar plot is not included because it is symmetric)

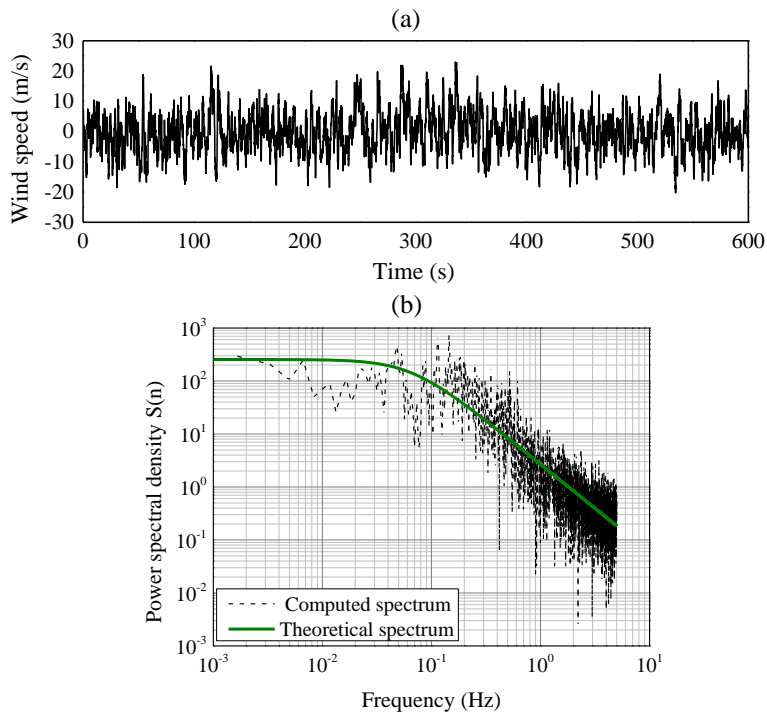


Fig. 4 Wind velocity simulation results: (a) wind velocity time-history and (b) computed and theoretical (Von Karman) wind spectra

Table 1 Summary of the parameters used in the wind velocity field simulation

Parameter	Model/Value
Type of geomorphology	Rural area
Mean velocity $U(z)$	$U(z)=U_{ref} ( z/Z_{ref} )^\eta$ where $z$ is height; $\eta=0.16$ (GB 50009-2012 2012); 10-min average wind velocity $U_{ref}=37.5, 42.5, 50, 55, 57$ (m/s) at the hub height of $Z_{ref}=65$ (CGC/GF 031:2013 2013, IEC 61400-3 2005).
Turbulence intensity $I_z$	$I(z)=I_{ref} ( z/Z_{ref} )^{-d}$ where $d=0.18$ (GB 50009-2012 2012); $I_{ref}$ increases by 0.02 from 0.16 at the reference height of the class A (IEC 61400-3 2005) to 0.18 (CGC/GF 031:2013 2013).
Turbulence length scale $L_u(z)$	$L_u(z)=L_u(ref) ( z/z_{ref} )^\gamma$ where $L_u(ref)=77$ (m); $z_{ref}=10$ (m); $\gamma=0.3$ , $u$ represents the longitudinal direction.
Turbulence power spectrum $S(f)$	$\frac{fS(f)}{\sigma_u^2} = \frac{4(fL_u(z)/U(z))}{(1+70.8(fL_u(z)/U(z))^2)^{5/6}}$ where $\sigma_u^2$ is the standard deviation of fluctuating velocity; $f$ is the frequency in Hz.
Coherency function	$Coh(f_m)=\exp(-C_j f dx_j / U(z))$ where $C_j=10$ is the coherency decay constant; $dx_j$ is the distance between the correlative points.
Other parameters	$f_{min}=0.01$ Hz, $f_{max}=10$ Hz are the minimum and maximum frequencies under consideration, respectively; $\Delta t=0.1$ s; $\Delta f=0.2$ Hz; $M=100$ ; $N=50$ ; $D=60$ ; $T=600$ s (IEC 61400-3 2005).

The proposed 1.5 MW WT is located in an area covered with a small amount of low shrubs, which corresponds to the geomorphic type “B” according to the code (GB 50009-2012 2012). With the parameters listed in Table 1, the wind velocity time-histories for the WT structure were constructed by using the CDRFG method. A typical 10-m-height record is shown in Fig. 4(a), and the computed spectrum produced by the CDRFG was compared with the theoretical von Karman spectrum in Fig. 4(b). It can be observed that the simulation is acceptable in terms of the frequency content. The wind velocity time histories along the wind turbine tower were estimated with the coherency function by discretizing the power spectra. The grid of the random wind speed field is generated along the height of the tower (Y axis) with an interval of 3-m (see L1-L20 in Fig. 2). At

the same elevation, the wind speed was assumed to be uniform (X and Z axes). For the wind load on blades and nacelle, the wind speed velocity time series were generated according to their spatial position (L21 and L22 in Fig. 2). These CDRFG generated transient wind velocity field data was used to estimate the wind loading applied in the dynamic analyses.

2.2.2 Wind load simulation

The wind loads on the WT tower, nacelle and hub, were calculated by using Eq. (1) and only along-wind load effects were considered in this study.

$$F(t) = 1/2 C_d \rho V^2(t) A \tag{1}$$

where  $\rho = 1.25 \text{ kg/m}^3$  is the air density;  $V(t)$  is the wind speed;  $C_d$  is the drag coefficient, which is 1.2 for a cylindrical shape structure (supporting tower and hub) or 1.3 for a rectangular shape body (nacelle), respectively; and  $A$  is the projection area.

The focus of this work is the structural response of the WT tower and not the detailed study of the wind-blade interaction. For this reason, the wind loading on the blades was estimated by the blade element momentum (BEM) theory (Hansen 2008). The blade was defined as a number of independent elements along its length. For a blade element, the force diagram represented in Fig. 5 can be drawn considering the wind velocities and actions. In this figure,  $V_{rel}$  is the effective wind velocity;  $\Omega$  is the rotational speed of a turbine blade and  $V_0$  is the incoming flow wind speed. In addition,  $r$  represents the distance from the cross-section to the centre of the hub. The parameters  $a$  and  $a'$  are the axial and tangential induction factors related to the blade geometry and wind speed, respectively.

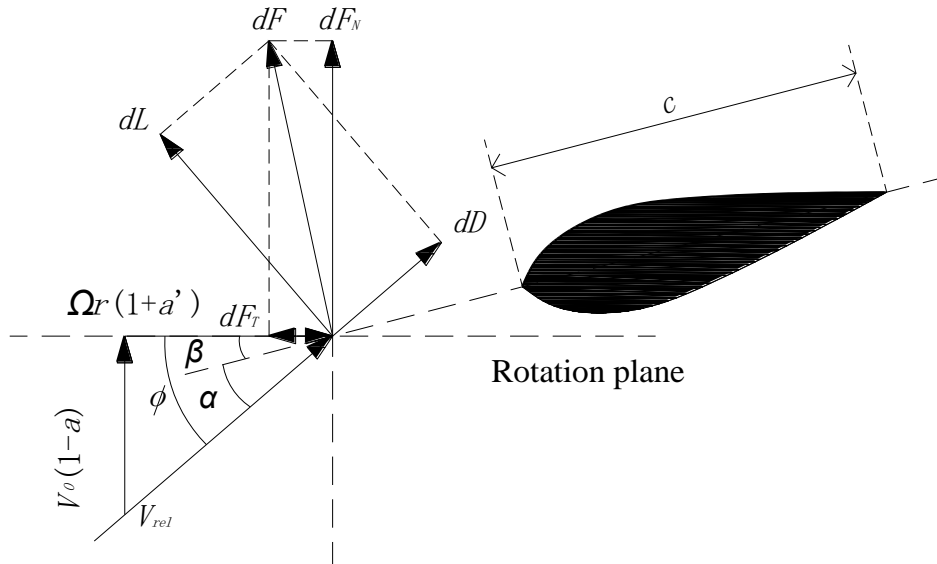


Fig. 5 Force and velocity diagram of a WT blade cross-section

The differential lift force  $dL$  or drag force  $dD$  per unit length, perpendicular or parallel to the relative velocity  $V_{rel}$ , respectively, were obtained as

$$\begin{cases} dL = 1/2\rho cV_{rel}^2 C_L \\ dD = 1/2\rho cV_{rel}^2 C_D \end{cases} \quad (2)$$

where  $C_L$  and  $C_D$  are the lift and drag coefficients of the blade, respectively;  $c$  is the blade's chord length.

The differential axial thrust force  $dF_N$  and rotary tangential force  $dF_T$ , which are respectively normal and tangential to the rotor-plane, can be derived with

$$\begin{cases} dF_N = dD \sin \phi + dL \cos \phi \\ dF_T = dL \sin \phi - dD \cos \phi \end{cases} \quad (3)$$

$$\phi = \alpha + \beta \quad (4)$$

where  $\phi$  is the inflow angle between the resultant wind velocity  $V_{rel}$  and the rotation plane;  $\alpha$  and  $\beta$  are the attack and the pitch angles, respectively.

The blade elements are assumed to be independent between each other, which allows to calculate the wind force on each strip separately. The total axial thrust force  $F_N$  and rotary tangential force  $F_T$  acting on the top of the WT tower result from the integration of these differential element forces, as shown in Eq. (5).

$$\begin{cases} F_N = \int_0^R dF_N dr \\ F_T = \int_0^R dF_T dr \end{cases} \quad (5)$$

where  $R$  is the length of the blade.

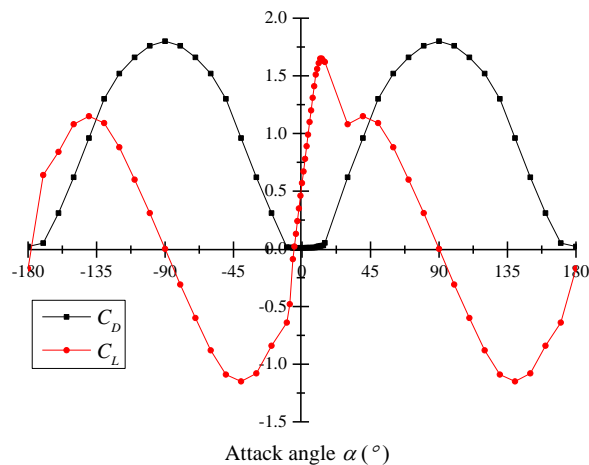


Fig. 6 Relationship between  $C_D$  ( $C_L$ ) and attack angle  $\alpha$

Table 2 Wind load estimation for a single blade under the unit wind speed, 0° inflow direction

Blade element	$r$ (m)	Chord length $c$ (m)	Pitch angle $\beta$ (°)	Attack angle $\alpha$ (°)	Drag coefficient $C_D$	Lift coefficient $C_L$	Drag force $dD$ (N)	Lift force $dL$ (N)	Thrust force $F_N$ (N)
1	1	2.44	89.66	0.34	0.009	0.604	0.03	1.84	0.03
2	3	2.32	88.99	1.01	0.009	0.671	0.03	1.95	0.03
3	5	2.21	88.31	1.69	0.009	0.745	0.02	2.06	0.02
4	7	2.09	87.64	2.36	0.009	0.820	0.02	2.14	0.02
5	9	1.97	86.97	3.03	0.009	0.893	0.02	2.20	0.02
6	11	1.85	86.29	3.71	0.010	0.961	0.02	2.23	0.02
7	13	1.74	85.62	4.38	0.010	1.032	0.02	2.24	0.02
8	15	1.62	84.94	5.06	0.010	1.106	0.02	2.24	0.02
9	17	1.50	84.27	5.73	0.010	1.173	0.02	2.20	0.02
10	19	1.38	83.60	6.40	0.011	1.244	0.02	2.15	0.02
11	21	1.26	82.92	7.08	0.011	1.318	0.02	2.08	0.02
12	23	1.15	82.25	7.75	0.011	1.385	0.02	1.99	0.02
13	25	1.03	81.57	8.43	0.012	1.453	0.01	1.87	0.01
14	27	0.91	80.90	9.10	0.013	1.515	0.01	1.73	0.01
15	29	0.79	80.23	9.77	0.018	1.549	0.02	1.54	0.02
16	31	0.68	79.55	10.45	0.021	1.582	0.02	1.34	0.02
17	33	0.56	78.88	11.12	0.022	1.615	0.02	1.13	0.02
Total	-	-	-	-	-	-	0.34	32.93	0.34

The 1.5-MW WT in this study consists of three blades each with a length of 34 m (Fig. 1). The chord length linearly decreases from 2.5 m at the base to 0.5 m at the tip of the blade. Each blade was divided into 17 segments with an element length of 2 m. The pitch angle of the blade  $\beta$  tapers linearly from 0.2 radians at the base to zero at the tip. The relationship between ( $C_L$ ) and the angle of attack  $\alpha$  (shown in Fig. 6) was obtained based on the S818 airfoil of the S-series airfoil families (Somers 2004).  $a$  and  $a'$  were assumed to be zero since they are very small in most cases.

It should be noted that, even with the aforementioned assumptions, it is difficult to simulate the wind load effects induced at the blades, especially for an operational condition of the WT. However, it is well accepted modern WTs are automatically shut down by the control system with a high wind speed when a typhoon is approaching (Ke *et al.* 2016). Under this shutdown scenario, the yaw and pitch system brake and the blades stop rotating (i.e.,  $\Omega=0$ ). Moreover, the blades are

usually adjusted into a “feather” state, resulting an approximate angle  $\alpha = 0^\circ$  between the chord axis and the inflow direction at the base of the blade, so that the frontal incoming flow wind loading can be reduced to the minimum. Thus the conventional scenario is the  $0^\circ$  inflow direction (shown in Fig. 1), in which the wind is perpendicular to the wheel plane along the fore-aft direction. An illustrative example of blade force estimation for a single blade based on the BEM under a unit wind speed and  $0^\circ$  inflow direction is provided in Table 2.

Considering the characteristic violent changes in the wind direction of TCs (Ishihara *et al.* 2005, Li *et al.* 2013, Wang *et al.* 2013), two additional inflow directions were investigated here in order to address the influence of the wind direction in the structural response, namely the  $90^\circ$ ,  $180^\circ$  wind inflow directions shown in Fig. 1. For the  $0^\circ$  and  $180^\circ$  inflow directions, the blade aerodynamic load is the total axial thrust load  $F_N$  from three blades. But at the inflow direction of  $90^\circ$ , the projected area of different blades associated with wind loads partially overlaps as shown in Fig. 1. In order to determine the wind loads on the wind wheel in this  $90^\circ$  inflow direction scenario, the approach of an integrated use of the BEM theory and the open-source program FAST, being developed based on multibody dynamics (Jonkman and Buhl 2005), was adopted. The single blade load tangential force  $F_T$  was first calculated based on the BEM theory; while in FAST, the aeroelastic wind load of the blade could be estimated by the shear force at the blade base. By comparing the maximum value of the total wind load from three blades, which was obtained from FAST, with the single blade load  $F_T$ , a parameter of 1.23 was determined.

Therefore, the blade aerodynamic load for the  $90^\circ$  inflow direction was estimated as the single blade load  $F_T$  times 1.23. By following this approach, the blade wind load estimations were achieved for different inflow directions. As expected, the  $90^\circ$  inflow direction is the most dangerous scenario: The ratio is 1: 69: 3 for the wind wheel forces at the  $0^\circ$ ,  $90^\circ$ ,  $180^\circ$  inflow directions, respectively. Nuta *et al.* (2011) observed a modest sensitivity of wind turbine tower response to the seismic loading direction, with a change in the pushover capacity of the wind turbine tower of only 10% for different incidence angles of the seismic action. Compared to earthquake ground motions, wind loads on the blades contribute more significantly to structural responses. The finding that the  $90^\circ$  inflow direction is a critical case was verified by simulations with different inflow winds by the authors and a similar conclusion was also reported in Wang *et al.* (2013).

The wind loads estimated for the WT tower as well as the blade wheel were distributed in 22 point loads along the height of the WT in the present study (“L1-L22” in Fig. 2). The surface of the tower was divided into 20 segments in order to apply the wind loads, considering the corresponding projected area and applying the load at its center according to Eq. (1). In order to apply the wind loading, a set of reference points were created in the FE model of the WT tower. Each reference point corresponds to the loading point along the height of the tower. This approach allows distributing uniformly wind loads corresponding to each tower segment. Additional wind loads were applied at the blade (L21) and the nacelle (L22) point masses, these simulate the wind load acting on the blades and the hub, as well as the nacelle, respectively. The blade wind loads were estimated following the method described aforementioned, while the hub and nacelle wind loading was calculated based on its projection area using Eq. (1). An initial analysis step was created to apply the gravity load in the numerical analysis, before the wind effects were considered.

The aforementioned approach calculates blade and tower loads separately, which is the basic philosophy for the equivalent static load method used in design codes and some research works (IEC-61400 2005, Gong and Chen 2015). This method may produce inaccurate results at extreme

wind condition, as the tower deforms significantly and the blade-tower interaction effects are considerable. However, since the primary objective of this study is to present the collapse process of the tower instead of an exact loading which this tower fails at, this simplified approach was adopted to save computational resources.

### 3. WT tower response analysis for different inflow directions

Several studies have observed that WT towers exhibit low damping levels (Hu *et al.* 2015). With the blades adjusted into a “feather” state during a strong wind event, only the structural damping was considered in this study, ignoring aerodynamic effects. The structural damping is defined as the 1% Rayleigh damping recommended by (IEC 61400-3 2005, ASCE 2011, Valamanesh and Myers 2014). The fundamental mode (0.49 Hz) and the 40<sup>th</sup> mode (23.11 Hz) were used to establish the Rayleigh damping. By including all the modes below the 40<sup>th</sup>, the cumulative modal mass activated in X-, Y-, and Z-direction is 91%, 75% and 91%, respectively. The input wind loading was constructed and applied to the FE model based on the method described in Section 2.2. To investigate structural responses and collapse modes, a total of 15 nonlinear time history analyses results were presented in this study. These are based on five different values of the 10-min average wind speed at the hub height,  $V_{hub}=37.5, 42.5, 50, 55, 57$  (m/s) (i.e.,  $U_{ref}$  in Table 1) provided by the wind turbine design codes (IEC 61400-3 2005, CGC/GF 031:2013 2013), with three different inflow directions (Fig. 1).

The maximum absolute values of the top acceleration and displacement as well as the base shear and moment from nonlinear time history analyses are summarized in Fig. 7. It is observed from the results that structural responses are similar when the inflow directions are 0° and 180°. At these two directions the tower is not heavily demanded even if the wind speed is as large as 57 m/s. However, the maximum wind speed that this particular tower can resist is less than 50 m/s when the inflow direction is 90°.

Four representative response time histories are shown in Fig. 8, corresponding to the cases with  $V_{hub}=50$  m/s at the hub. It should be noted that structural collapse occurred approximate 162s after the start of the simulation for the 90° inflow direction, beyond which the numerical analysis did not converge due to excessive structural deformation. The results in Fig. 8 verify that the absolute values of structural response are almost coincident for 0° and 180° inflow directions.

Figs. 7 and 8 illustrate that the response of the WT tower is significantly larger when the wind inflow direction is 90°, in comparison with the other two directions. The power response acceleration spectra for the case with  $V_{hub}=37.5$  m/s is included in Fig. 9 for different inflow directions. They all present a clear peak at 0.49 Hz, which corresponds to the 1<sup>st</sup> global flexure mode shown in Fig. 3 and demonstrates that the structural response is governed by the fundamental mode of the tower when it is subject to wind actions. However, the 90° inflow direction exacerbates the response amplitude. The same findings can be observed for the displacement, base shear and base bending moment as well. The reason is attributed to the fact that (1) the wind load transmitted from the blades to the WT wall significantly increases for the 90° inflow direction, and (2) the projected area of the nacelle in this direction is larger, which increases the wind load in this part of the WT (Wang *et al.* 2013).

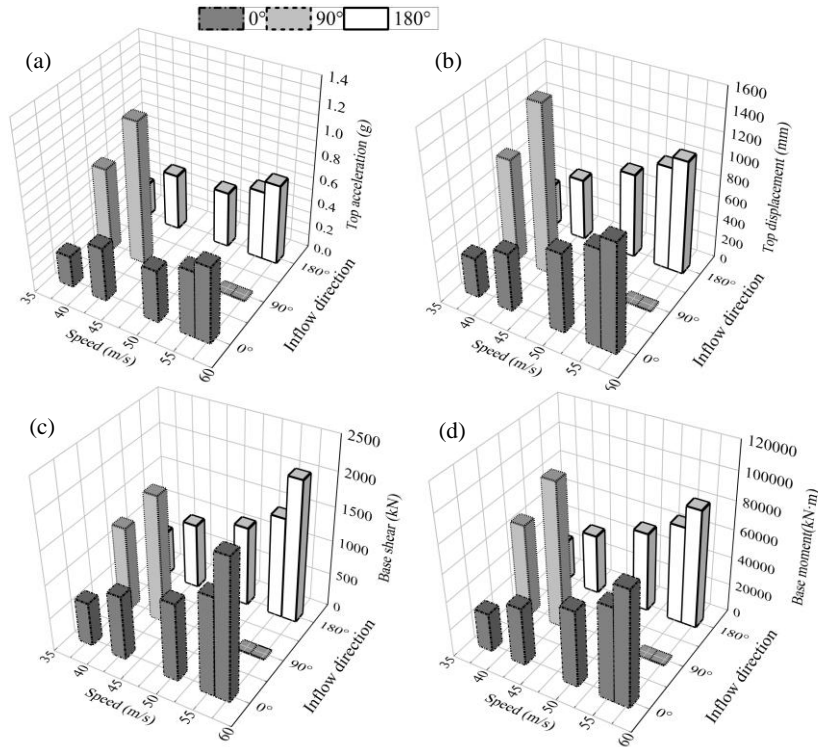


Fig. 7 Maximum (absolute) values of the structural responses in nonlinear dynamic analyses: (a) top acceleration, (b) top displacement, (c) base shear, and (d) base moment. Note: when no data is represented in the bar plots, it represents that tower collapses during the analysis

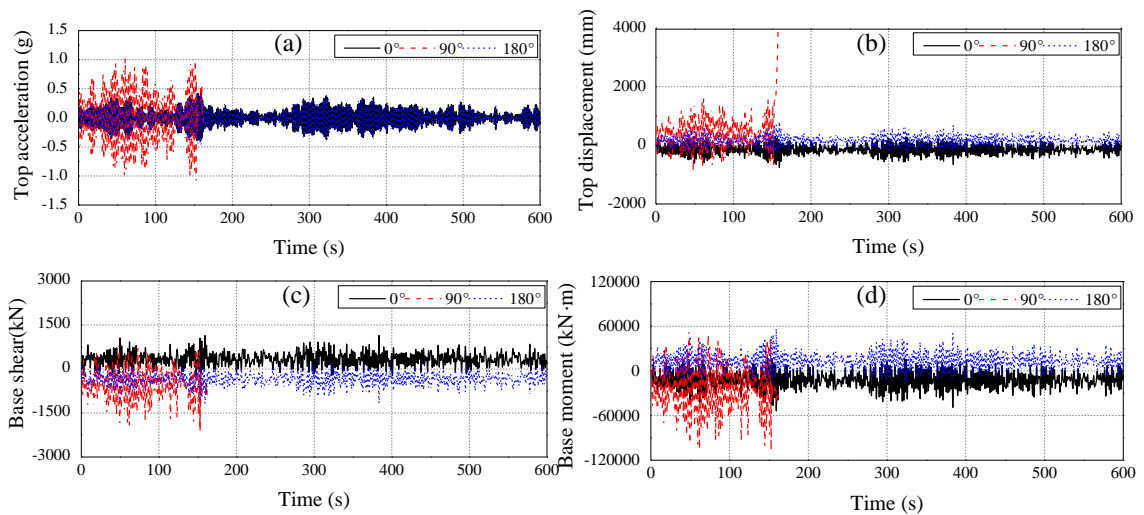


Fig. 8 Nonlinear response time histories: (a) top acceleration, (b) top displacement, (c) base shear, and (d) base moment for  $V_{hub}=50$  m/s and inflow directions of  $0^\circ$ ,  $90^\circ$ ,  $180^\circ$

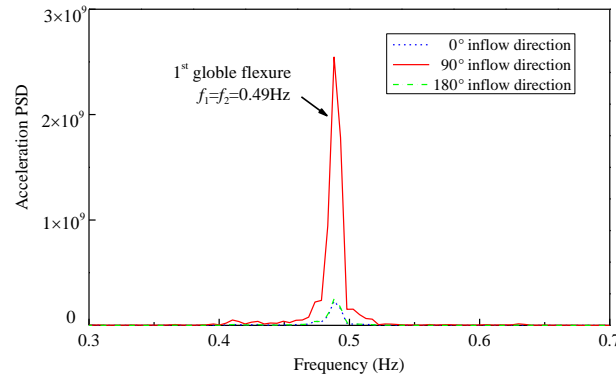


Fig. 9 Acceleration power spectral densities of structural responses at the tower top for  $V_{hub}=37.5$  m/s and inflow directions of  $0^\circ$ ,  $90^\circ$ ,  $180^\circ$

## 4. Buckling and collapse mode analyses

### 4.1 Eigenvalue buckling analysis

A linear eigenvalue buckling analysis was first performed in order to obtain a first approximation of the capacity of the WT tower. The first four buckling modes are shown in Fig. 10. It can be observed that the first three buckling modes involve the deformation of the wall around the entrance door. After these, the fourth buckling mode is localized at the middle ring of the WT tower, at a distance that ranges from 34.6 to 36.9 m from the tower base. The applied initial buckling load was normalized with the square of wind speed, which results in a wind speed of 200 m/s (i.e.,  $\sqrt{40066}$ ), corresponding to the critical load factor  $\lambda_1$ . This wind speed is considered the upper bound of the ultimate buckling load in previous works (Jaca *et al.* 2007). The ratio between the critical wind speed in the buckling analysis and the collapse wind speed obtained with nonlinear dynamic analysis (50 m/s in Section 3) is 4.0. This result clearly indicates that the eigenvalue buckling analysis gives an unsafe estimation of the ultimate load. Interestingly, the ratio between the ultimate wind speed in dynamic and eigenvalue analysis falls in the range between 3 to 5, which is in agreement with the empirical observations in other thin cylindrical shell structures (Karman and Tsien 1941).

### 4.2 Collapse mode analysis

A typical total of 15 nonlinear time history analyses were presented with five different wind speeds and three different wind inflow directions. Table 3 presents the initial plastic hinge locations along the tower and the corresponding time instants for the  $90^\circ$  inflow direction under the five different wind speeds. The  $0^\circ$  and  $180^\circ$  inflow direction cases were not presented in the Table 3 since there is no plastic hinges within the analysis scope. Considering the  $90^\circ$  inflow direction, it was found that the yielding in the steel wall arises when the mean wind exceeds 42.5 m/s (Zhang *et al.* 2014, Chen *et al.* 2015). The locations at which the plastic hinges develop depend on the wind speed, being usually located between 0 and 23 m ( $H/3$ ) from the base, i.e.,

within the bottom third of the tower height, which is consistent with the observations reported in previous cylindrical shell studies (Pircher *et al.* 2009). This suggests the validity of the proposed nonlinear dynamic analysis for the assessment of WT farms under cyclonic winds and the need for further research on its use for this kind of analysis. It should be also noted that the instant corresponding to the occurrence of the initial plastic hinge is generally delayed by decreasing the wind speed.

Figs. 11-13 present the displacement time-histories of the tower top and the corresponding von Mises stress distribution for the cases with  $V_{hub}=50$  m/s, 55 m/s, 57 m/s, in the  $90^\circ$  inflow direction, respectively. Different response stages were observed throughout the entire time-history analyses: (i) initial plastic hinge formation; (ii) formation of full-section plastic hinges; (iii) complete collapse. Here, the complete collapse was assumed to be associated with a tower top displacement of approximately 6-7 m in the FE model responses. The collapse mode observed in nonlinear dynamic analyses significantly differs from the linearized buckling analysis. Instead of the locations close to the door in which the first three buckling modes are concentrated in Fig. 10, in the nonlinear dynamic time history analyses, the full-section plastic hinges were located at the height of 8.8 m or 11.8 m for  $V_{hub}=50$  m/s,  $V_{hub}=55$  m/s (and  $V_{hub}=57$  m/s), respectively. These locations are clearly above the door level, and below the sections corresponding to the buckling according to the fourth eigenmode in Section 4.1. It is also noted that the start of the development of the plastic hinge and its full formation occur at different instants under different intensities of the wind load.

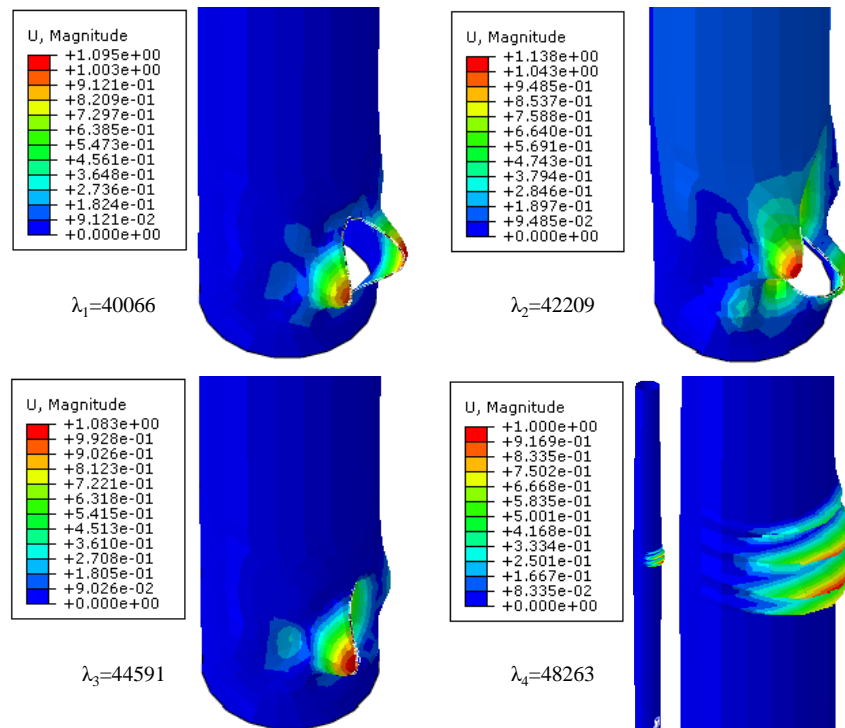


Fig. 10 First four buckling modes and corresponding load factors in the WT wall (Note: deformations are enlarged 900 times)

Table 3 Initial plastic hinge locations and the corresponding time instants

Extreme wind speed $V_{hub}$ (m/s)	Inflow direction	
	90°	
	Location	Time(s)
37.5	-	-
42.5	A C D E F G H I J	277
50	A C D E F	59.5
55	C D E	6.1
57	A C D E F G H I	12.2

\*Note: "-" represents no plastic hinge

For example, considering  $V_{hub} = 57$  m/s (Fig. 13), the full-section plastic hinge formation closely follows the initiation of a plastic hinge; however, for  $V_{hub} = 50$  m/s (Fig. 11) it takes more than 90s to reach full-section plasticity after the initiation of the plastic hinge. The numerical simulation shows that WT towers are consequently very sensitive to the formation of the plastic hinge because of the lack of structural redundancy in the tower wall. The structure rapidly collapses once a single full-section plastic hinge is fully formed under strong wind conditions.

For all the cases in this collapse simulation, the failure positions are located between the height 8.8 m and 11.8 m, which is approximately  $H/5 \sim H/7$  above the tower base. This position is higher than the door opening. Similar findings were reported in forensic studies of WT failures (Chen *et al.* 2015, Chen and Xu 2016).

It should be emphasized that even though the formation of the initial plastic hinge differs along the tower for various wind speeds, the full-section plastic hinge is only formed by developing one of the initial plastic hinges along the tower wall. The collapse region is determined by the location of this full-section plastic hinge.

In order to gain insight on the energy balance during the dynamic response analysis of the WT tower, Fig. 14 compared the energy dissipated by structural plasticity at the hinges developing along the wall and also by structural viscous damping. Both the non-failure (Figs. 14(a) and 14(d)) and collapse (Figs. 14(b) and 14(c)) scenarios were compared, observing significant differences. When the wind loading is below the critical value that induces failures, the external energy introduced by the wind is almost entirely dissipated by structural viscous damping, as shown in Figs. 14(a) and 14(d) (non-failure scenarios).

However, when the wind load is above the level associated with collapse, almost all the input energy is invested in the plastic dissipation at the hinge. In these cases the stages of collapse can be clearly appreciated in the evolution of the plastic dissipation in Figs. 14(b) and 14(c), corresponding with the sequential stages in the plastic hinge development.

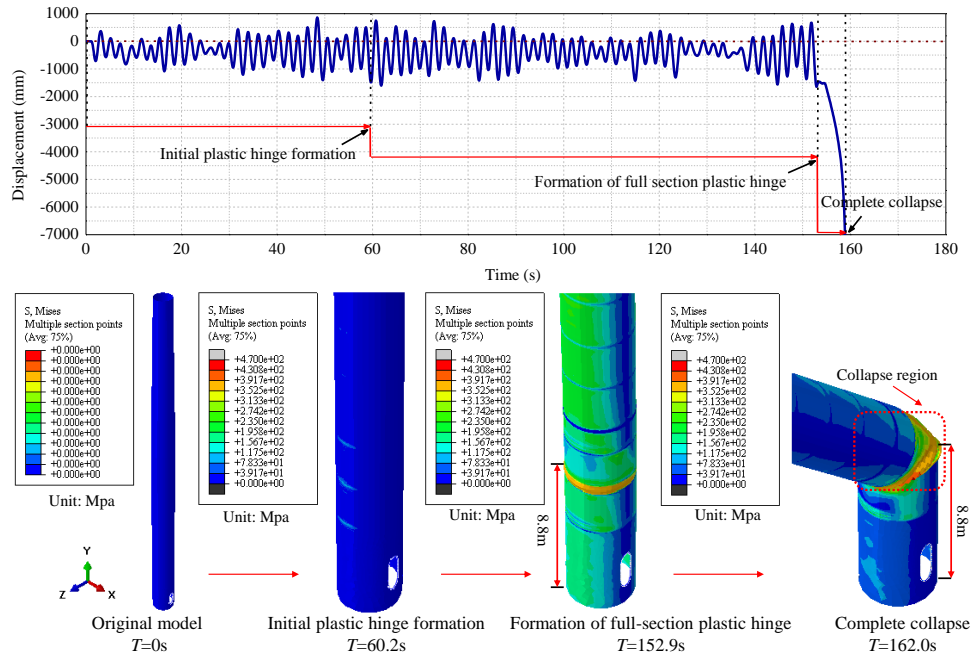


Fig. 11 Top displacement time history and the corresponding von Mises stress (MPa) distribution of FE model for the loading case of  $V_{hub}=50$  m/s,  $90^\circ$  inflow direction

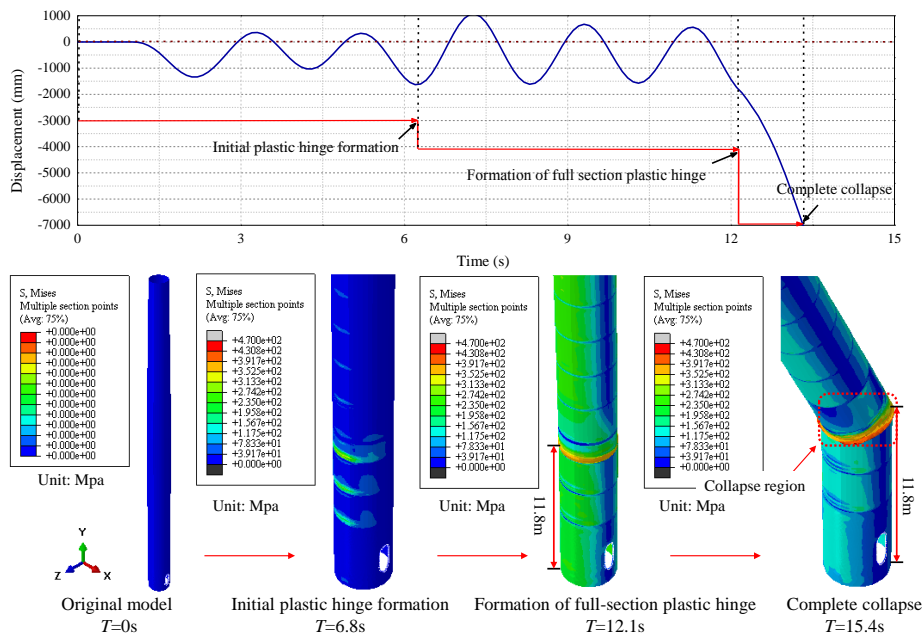


Fig. 12 Top displacement time history and the corresponding von Mises stress (MPa) distribution of FE model for the loading case of  $V_{hub}=55$  m/s,  $90^\circ$  inflow direction

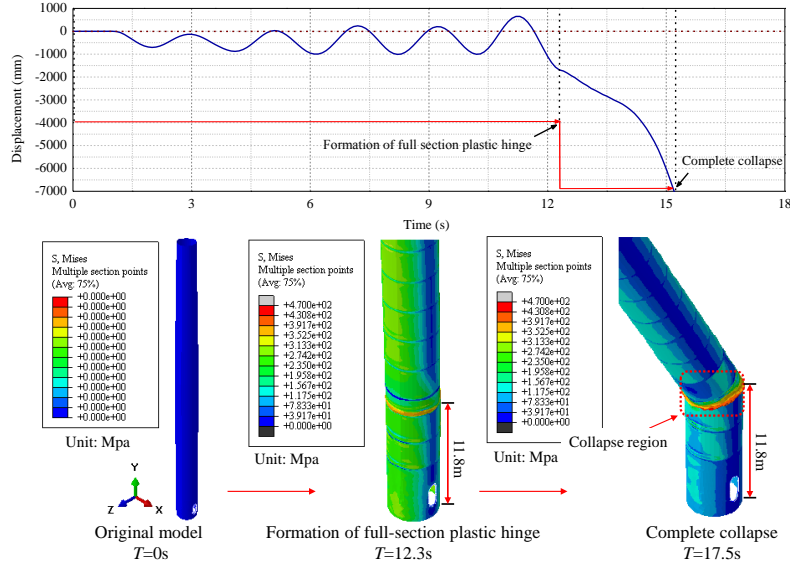


Fig. 13 Top displacement time history and the corresponding von Mises stress (MPa) distribution of FE model for the loading case of  $V_{hub}=57$  m/s,  $90^\circ$  inflow direction

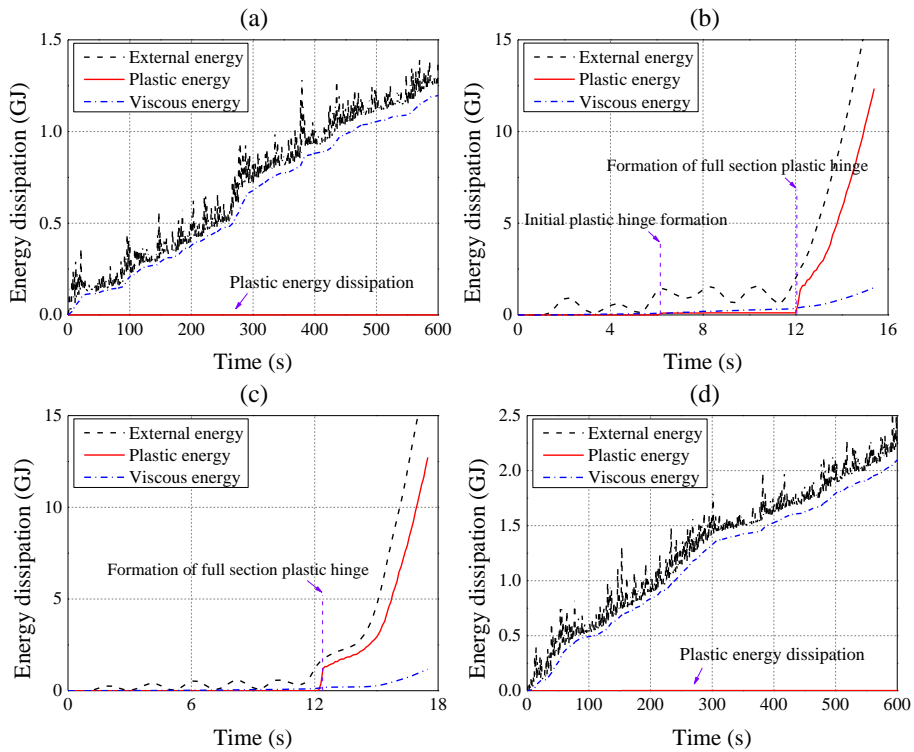


Fig. 14 Energy dissipation time histories for four cases: (a)  $V_{hub}=50$  m/s,  $0^\circ$  inflow direction, (b)  $V_{hub}=50$  m/s,  $90^\circ$  inflow direction, (c)  $V_{hub}=55$  m/s,  $90^\circ$  inflow direction and (d)  $V_{hub}=55$  m/s,  $180^\circ$  inflow direction

The current research demonstrates that the nonlinear dynamics analysis is recommended if detailed collapse forensic engineering research is required, although it is computationally expensive. On the other hand, the linear elastic analysis should be adequate for most structural analyses (Jonkman and Buhl 2005, Chou and Tu 2011). Moreover, it should be noted that the random nature of wind loads and modeling uncertainties of the wind turbine tower may affect simulation results and the findings above may not be exactly the same for different simulations. Due to the heavy computational demands of nonlinear analysis, extensive calculations were not included herein. However, as the focus of this study is to present a failure process of the wind turbine tower, the typical structural responses and failure cases described in this study should be of interest to the structural engineering community of wind industry, which were not reported in those aftermath field investigations such as Chen and Xu (2016).

## 5. Conclusions

A 1.5MW WT tower under cyclone wind loading actions was studied in this paper. A detailed FE model of this 61.8 m tall tubular steel tower was established and 15 along-wind load time-histories were generated for different speed levels and inflow directions. The consistent discrete random flow generation method was employed in the generation of the tropical cyclone wind velocity histories. The following conclusions were obtained from the numerical simulations:

- The nonlinear dynamic analysis of the WT tower under strong tropical cyclone wind allows to distinguish the following failure stages in the time-history response of the structure: (i) initial plastic hinge formation; (ii) full-section plastic hinge formation; (iii) complete collapse. Further research is needed to improve the structural design in order to prevent or delay the occurrence of the different stages of the collapse sequence.
- In the idle condition with the  $0^\circ$  angle between the chord axis and the inflow direction at the base of the blades, the flow direction ( $0^\circ$  and  $180^\circ$ ) makes a small difference in the structural response as the wind flow is perpendicular to the blade's wheel plane. However, when the wind is parallel to this plane ( $90^\circ$ ), the situation is critical for the structural response, due to the large wind forces on the blades and the nacelle. The power response acceleration spectra in this scenario shows a large amplification corresponding to the contribution of the first vibration mode of the tower.
- Plastic hinges are initiated along the tower wall in sections located in the first third of the tower, from 0 to 23 m ( $H/3$ ) above its base. A single full-section plastic hinge is sufficient to cause the structural collapse. There is a delay between the onset of plasticity in the wall and the full plastic hinge development, which was captured with nonlinear material and geometric finite element analysis of the wall discretized with shell elements. The full hinges have been observed at heights of 8.8~11.8 m from the base in this tower, i.e.,  $H/5\sim H/7$ , which were also reported as failure locations in previous forensic case studies.
- The linearized eigenvalue buckling analysis suggests failure modes that mainly involve the deformation around the opening door. However, this was not observed in the nonlinear dynamic analysis, in which failure occurs after the formation of an initial plastic hinge along the tower height. Previous field observations are in agreement with the proposed nonlinear time-history analysis, which is recommended in the assessment of the wind turbine response under strong wind excitations.

## Acknowledgments

The authors would like to acknowledge supports from the State Key Laboratory of Disaster Reduction in Civil Engineering (SLDRCE14-B-02), State Key Laboratory for GeoMechanics and Deep Underground Engineering (SKLGDUEK1514), State Key Laboratory of Geohazard Prevention and Geoenvironment Protection (SKLGP2016K006), Key Laboratory of Energy Engineering Safety and Disaster Mechanics, Ministry of Education (Grant No. EES201603), Science and Technology Commission of Shanghai Municipality International Collaboration Program (16510711300), and China National Key R & D Program (Special Key Program for International Cooperation, 2016YFE0105600).

## References

- ABAQUS (2013), Abaqus 6.13\_1 analysis user's manual, Dassault Systèmes Simulia Corp, Providence, RI, USA.
- Aboshosha, H., Elshaer, A., Bitsuamlak, G.T. and Damatty, E.A. (2015), "Consistent inflow turbulence generator for LES evaluation of wind-induced responses for tall buildings", *J. Wind Eng. Ind. Aerod.*, **142**, 198-216.
- An, Y., Quan, Y. and Gu, M. (2012), "Field measurement of wind characteristics of typhoon Muifa on the Shanghai world financial center", *Int. J. Distrib. Sens. N.*, **2012**, 1-11.
- ASCE/AWEA (2011), Recommended practice for compliance of large land-based wind turbine support structures, American Society of Civil Engineers/American Wind Energy Association; Reston, USA.
- Chen, X., Li, C. and Xu, J. (2015), "Failure investigation on a coastal wind farm damaged by super typhoon: A forensic engineering study", *J. Wind Eng. Ind. Aerod.*, **147**, 132-42.
- Chen, X. and Xu, J.Z. (2016), "Structural failure analysis of wind turbines impacted by super typhoon Usagi", *Eng. Fail. Anal.*, **60**, 391-404.
- Choi, E.C.C. (1978), "Characteristics of typhoons over the South China Sea", *J. Wind Eng. Ind. Aerod.*, **3**(4), 353-365.
- Chou, J.S. and Tu, W.T. (2011), "Failure analysis and risk management of a collapsed large wind turbine tower", *Eng. Fail. Anal.*, **18**, 295-313.
- CGC/GF 031:2013 (2013), Simulation design code for typhoon wind turbine, Beijing Jianheng technical specification; Beijing, China. (in Chinese)
- Dai, K.S., Bergot, A., Liang, C., Xiang, W.N. and Huang, Z.H. (2015), "Environmental issues associated with wind energy- A review", *Renew. Energ.*, **75**, 911-921.
- Dai, K.S., Huang, Y.C., Gong, C.Q., Huang, Z. and Ren, X.S. (2015), "Rapid seismic analysis methodology for in-service wind turbine towers", *Earthq. Eng. Eng. Vib.*, **14**, 539-548.
- Field, C.B. (Ed.) (2012), *Managing the Risks of Extreme Events and Disasters to Advance Climate Change Adaptation*, Cambridge University Press, Cambridge, UK, and New York, NY, USA.
- GB/T 31519-2015 (2015), Wind turbine generator system under typhoon condition, Standards Press of China; Beijing, China. (in Chinese).
- GB 50009-2012 (2012), Load code for the design of building structures, Architecture and Building Press; Beijing, China. (in Chinese)
- GL (2005), Guidelines for certification of offshore wind turbines, Germanischer Lloyd; Hamburg, Germany.
- Gong, K. and Chen, X. (2015), "Improved modeling of equivalent static load on wind turbine towers", *Wind Struct.*, **20**(5), 609-622.
- Hansen, M.O.L. (2008), *Aerodynamics of wind turbines*, 3<sup>rd</sup>Ed., Earthscan, London, UK.
- Han, T., McCann, G., Mücke, T.A. and Freudenreich, K. (2014), "How can a wind turbine survive in tropical cyclone?", *Renew. Energ.*, **70**, 3-10.

- Hu, W.H, Thöns, S., Rohrmann, R.G., Said, S. and Rücker, W. (2015), "Vibration-based structural health monitoring of a wind turbine system Part II: Environmental/operational effects on dynamic properties", *Eng. Struct.*, **89**, 273-90.
- IEC 61400-1 (2005), Wind Turbines - Part 1: Design Requirements, Geneva, Switzerland.
- Ishihara, T., Yamaguchi, A., Takahara, K., Mearu, T. and Matsuura, S. (2005), "An analysis of damaged wind turbines by typhoon maemi in 2003", *Proceedings of the 6th Asia-Pacific Conference on Wind Engineering*, Seoul, Korea, September, 12-14.
- Jaca, R.C., Godoy, L.A., Flores, F.G. and Croll, J.G.A. (2007), "A reduced stiffness approach for the buckling of open cylindrical tanks under wind loads", *Thin Wall. Struct.*, **45**, 727-736.
- Jonkman, J.M. and Buhl, M.L. (2005), FAST User's Guide, National Renewable Energy Laboratory, Golden, USA.
- Ke, S.T., Yu, W., Wang, T.G., Zhao, B., and Ge, Y.J. (2016), "Wind loads and load-effects of large scale wind turbine tower with different halt positions of blade", *Wind Struct.*, **23**(6), 559-575.
- Karman, T. and Tsien, H.S. (1941), "The buckling of thin cylindrical shells under axial compression", *J. Aeronaut. Sci.*, **8**(8), 303-312.
- Lavassas, I., Nikolaidis, G., Zervas, P., Efthimiou, E., Doudoumis, I.N. and Baniotopoulos, C.C. (2003), "Analysis and design of the prototype of a steel 1-MW wind turbine tower", *Eng. Struct.*, **25**, 1097-1106.
- Lee, K.S. and Bang, H.J. (2012), "A study on the prediction of lateral buckling load for wind turbine tower structures", *Int. J. Precision Eng. Manufacturing*, **13**(10), 1829-1836.
- Li, Z.Q., Chen, S.J., Ma, H. and Feng, T. (2013), "Design defect of wind turbine operating in typhoon activity zone", *Eng. Fail. Anal.*, **27**, 165-172.
- Nuta, E., Christopoulos, C. and Packer, J.A. (2011), "Methodology for seismic risk assessment for tubular steel wind turbine towers: application to Canadian seismic environment", *Can. J. Civil Eng.*, **38**(3), 293-304.
- Patil, A., Jung, S. and Kwon, O.S. (2016), "Structural performance of a parked wind turbine tower subjected to strong ground motions", *Eng. Struct.*, **120**, 92-102.
- Pircher, M., Lechner, B. and Trutnovsky, H. (2009), "Elastic buckling of thin-walled cylinders under wind loading: An experimental study", *Int. J. Struct. Stab. Dynam.*, **9**, 1-10.
- Sadowski, A.J., Camara, A., Málaga-Chuquitaype, C. and Dai, K.S. (2016), "Seismic analysis of a tall metal wind turbine support tower with realistic geometric imperfections", *Earthq. Eng. Struct. D.*, DOI: 10.1002/eqe.2785.
- Shiau, B.S. and Chen, Y.B. (2001), "In situ measurement of strong wind velocity spectra and wind characteristics at Keelung coastal area of Taiwan", *Atmos. Res.*, **57**, 171-185.
- Spagnoli, A. and Montanari, L. (2013), "Along-wind simplified analysis of wind turbines through a coupled blade-tower model", *Wind Struct.*, **17**(6), 589-608.
- Somers, D.M. (2004), "The S816, S817, and S818 Airfoils", Research Report No. AF-1-11154-1 National Renewable Energy Laboratory, Colorado, Pennsylvania, USA.
- Sultania, A. and Manuel, L. (2016), "Loads and motions for a spar-supported floating offshore wind turbine", *Wind Struct.*, **22**(5), 525-541.
- Valamanesh, V. and Myers, A. (2014), "Aerodynamic damping and seismic response of horizontal axis wind turbine towers", *J. Struct. Eng. - ASCE*, **140**, 1-9.
- Vickery, P.J., Wadhwa, D., Powell, M.D. and Chen, Y. (2009), "A hurricane boundary layer and wind field model for use in engineering applications", *J. Appl. Meteorol. Clim.*, **48**, 381-405.
- Wang, Z., Zhao, Y., Li, F. and Jiang, J. (2013), "Extreme dynamic responses of MW-level wind turbine tower in the strong typhoon considering wind-rain loads", *Math. Probl. Eng.*, **2013**, 1-13.
- WWEA (2016), The world sets new wind installations record: 63,7 GW NEW CAPACITY IN 2015; World Wind Energy Association, Bonn, Germany. <http://www.windea.org/the-world-sets-new-wind-installations-record-637-gw-new-capacity-in-2015/>
- Zhang, Z., Li, J. and Zhuge, P. (2014), "Failure analysis of large-scale wind power structure under simulated typhoon", *Math. Probl. Eng.*, **2014**, 1-10.

100 *Kaoshan Dai, Chao Sheng, Zhi Zhao, Zhengxiang Yi, Alfredo Camara and Girma Bitsuamlak*

*AD*